Electronic Supplementary Material (ESI) for Journal of Materials Chemistry C.

Super-tough and self-healing biomimetic luminescent elastomer enabled by hydrogen bonding arrays and lanthanide-bipyridine moieties

Di Zhao [a], Chunmei Yue [a], Qianrui Li [a], Lei Guo [a] and Huanrong Li [a]*

[a] School of Chemical Engineering and Technology, Hebei University of Technology, GuangRong Dao 8, Hongqiao District, Tianjin 300130, P. R. China.

Corresponding author: E-mail: lihuanrong@hebut.edu.cn

Experimental section

1. Materials

Unless otherwise specified, all reactants and solvents are commercial and have not been further purified. Adipic dihydrazide (AD), tolylene-2,4-diisocyanate-terminated polypropylene glycol (PPG-NCO; Mn ≈ 2300) and dibutyltin dilaurate (DBTDL, 95%) were purchased from Sigma-Aldrich. [2,2'-Bipyridine]-4,4'-dimethanol (Bpy-OH) was obtained from Beijing Warwick Chemical Co., Ltd. N, N-dimethylformamide (DMF) was purchased from Kemat (Tianjin) Chemical Technology Co., Ltd.

2. Synthesis of APU-$Bpy_{0.1}$-Ln:

AD (0.9 mmol) powder and DBTDL (10 μL) were dispersed in 5 mL DMF solvent under magnetic stirring at 80 °C, then, PPG-NCO (1 mmol) dissolved in DMF (10 mL) was added to the above system after the AD powder was completely dissolved, and further stirred at 80 °C for 10 min. The product obtained in this step was noted as **APU**. Then, Bpy-OH (0.1 mmol) dispersed in 5 mL DMF was dropped into the above solution, and then the solution was stirred for 6 h at 80 °C. The polymer-ligands of this step were denoted as **APU-$Bpy_{0.1}$** (Mn=15041 g/mol, Mw=20287 g/mol, see **Figure S19**). Afterward, the $LnCl_3 \cdot 6H_2O$ (Ln^{3+}: Eu^{3+} and/or Tb^{3+}, 0.333 mL, 0.1 mol L^{-1}) was added into the **APU-$Bpy_{0.1}$** mixture with stirring for 1 hour at room temperature to coordinate Ln^{3+} with the polymer-ligands. The obtained solution was then cast into glass petri dishes at 80 ℃ for 48 h to the constant weight. The obtained films are noteed as **APU-$Bpy_{0.1}$-Ln** with a thickness of approximately 0.4 mm. Adjusting the feed ratios of the raw materials, a series of samples with various n values was synthesized through

a similar process. The feed ratios of various **APU-Bpy$_n$-Ln** (n=0.5, 0.4, 0.3, 0.2, 0.1, 0.05, 0) are summarized in **Table S1**.

3. Characterizations

Fourier transform infrared (FT-IR) measurements were examined on the Bruker TENSOR 27 spectrometer in the range of 400−4000 cm^{-1} (16 scans, resolution: 4 cm^{-1}). Temperature-dependent FT-IR spectra was evaluated on Tensor 27 in the range of 400−4000 cm^{-1}. Stress-strain curves were obtained on the CMT6104 with a stretch speed of 100 mm min^{-1}, the gauge length, width and thickness of the samples were about 10, 5 and 0.4 mm respectively, each test was conducted at least 5 times. For cyclic tensile tests, the maximum strain was set to be 100% (for different strains: 20%, 40%, 80%, 160%, 320% and 640%) and appropriate consecutive cycles were conducted out. The transmittance spectra were tested on Agilent Cary 100 UV-Vis spectrometer. Differential scanning calorimetry (DSC) was evaluated on a TA DSC Q2000 differential scanning calorimeter in the range of −80 °C-200 °C with a heated or cooled rate of 10 °C/min in the atmosphere. The gel permeation chromatography (GPC) was recorded by Agilent PL-GPC50 and THF was taken as the mobile phase. Rheological performances measurements were obtained on an Anton Paar MCR302 rheometer under ambient conditions. Frequency sweeps measurements were tested from 0.068 to 628 rad/s under 1% strain. Strain sweeps curve was tested with a strain of 0.001-1000% at 25 °C (frequency:1 Hz). Wide-angle X-ray diffraction (WAXD) pattern was determined by a Bruker AXS D8 Discover X-ray diffractometer. Thermal gravimetric analysis (TG) was measured on America TA 209 SDT/Q600 instrument in the range of

25-800 °C under nitrogen atmosphere with a heating rate of 10 °C min^{-1}. Small-angle X-ray scattering (SAXS) measurements were carried out on a Bruker NanoSTAR system and Cu Kα radiation (λ = 0.1541 nm) was used as the X-ray source. The absolute quantum yields were carried out with a barium sulfate-coated integrating sphere (150 mm in diameter) linked to the FS920P. Lifetime tests and steady-state luminescence spectroscopy were evaluated by Edinburgh Instruments FS920P spectrometer. Dynamic mechanical analyses (DMA) were obtained on DMA Q800 V21.1 Build 51 at a frequency of 1Hz. ^{1}H NMR spectra were evaluated on the Bruker AVANCE III HD500 spectrometer.

Sample	PPG-NCO (mg/mmol)	AD (mg/mmol)	Bpy-OH (mg/mmol)	Ln^{3+} (mL/mmol)
APU-Bpy_0	2.3/1	174/1	0	0
APU-$Bpy_{0.05}$-Ln	2.3/1	165/0.95	11/0.05	0.167/0.0167
APU-$Bpy_{0.1}$-Ln	2.3/1	156.6/0.9	21.6/0.1	0.333/0.0333
APU-$Bpy_{0.2}$-Ln	2.3/1	139.2/0.8	43.2/0.2	0.666/0.0666
APU-$Bpy_{0.3}$-Ln	2.3/1	121.8/0.7	64.8/0.3	1/0.1
APU-$Bpy_{0.4}$-Ln	2.3/1	104.4/0.4	86.4/0.4	1.333/0.1333

Table S1. The feed ratios of various **HMPU-Tpy_n-Ln**.

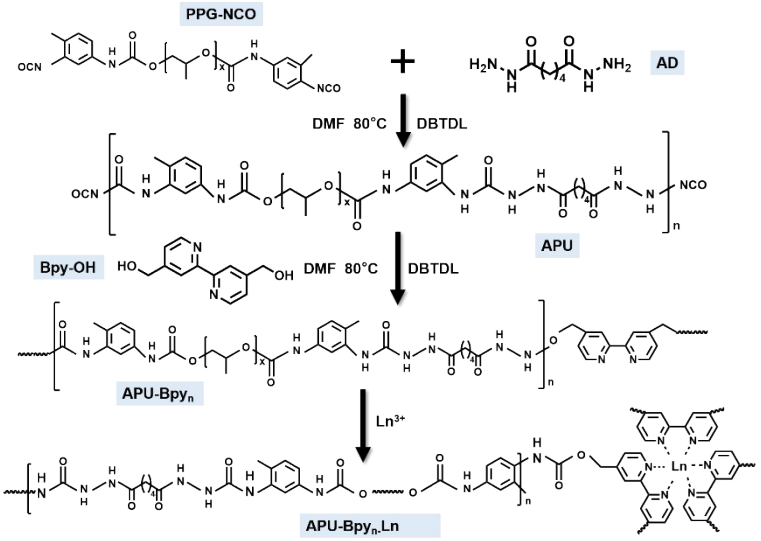

Figure S1. Synthetic route of **APU-Bpy_n-Ln**.

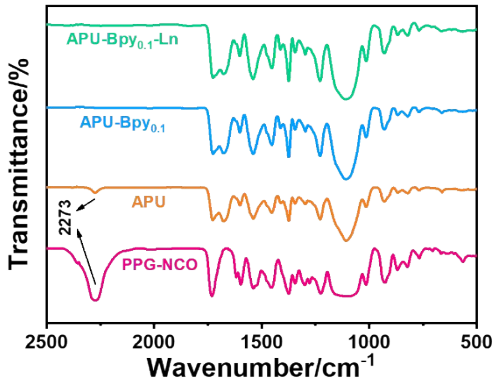

Figure S2. FT-IR spectra of a series of products.

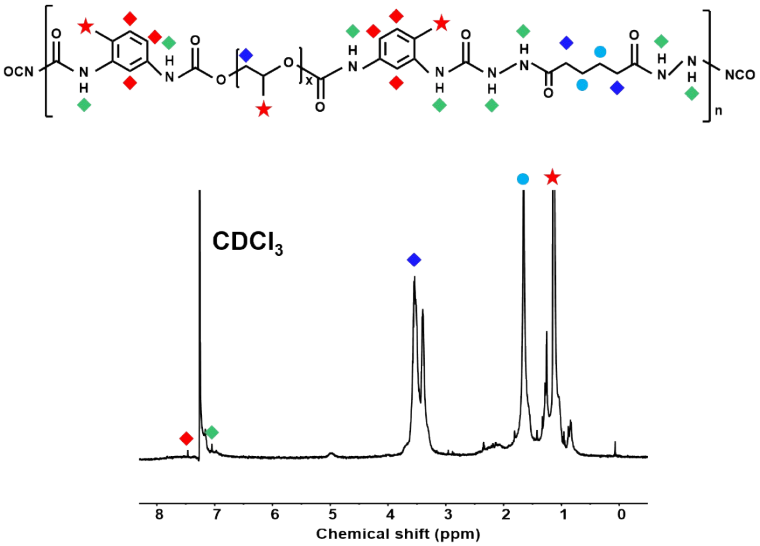

Figure S3. ^{1}H NMR spectrum (500 MHz, $CDCl_3$, room temperature) of **APU**.

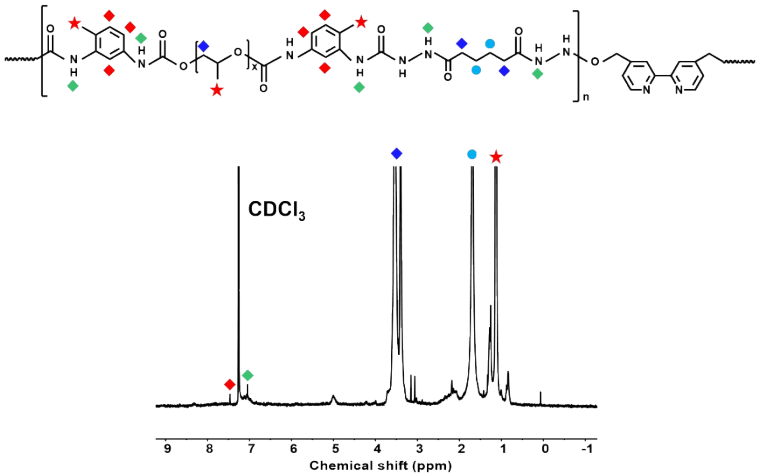

Figure S4. ^{1}H NMR spectrum of **APU-Bpy$_{0.1}$**.

NMR signal of H atoms of Bpy do not appears in **Figure S4** because its

concentration is too low to be detected.[1] Based on the above, we have demonstrated successfully synthesis of **APU-Bpy$_{0.1}$** via FT-IR (**Figure S2**).

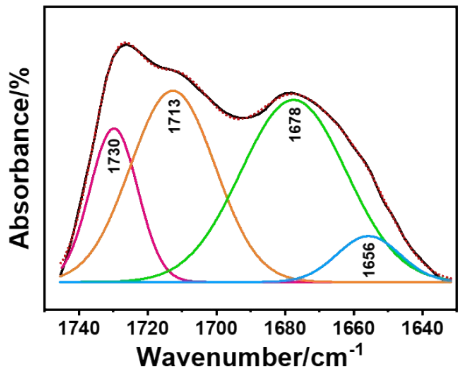

Figure S5. FT-IR absorption spectra in the C=O stretching region (1745~1631 cm^{-1}) of the obtained **APU-Bpy$_{0.1}$-Ln** material. The four fitted bands at 1730, 1713, 1678 and 1656 cm^{-1}, respectively.

These four peaks of **APU-Bpy$_{0.1}$-Ln** in (1745~1631 cm^{-1}) belong to free C=O (1730 cm^{-1}, 15.97%), H-bonded in urethane C=O (1713 cm^{-1}, 35.52%), disordered H-bonded C=O in urea (1678 cm^{-1}, 42.21%) and ordered H-bonded C=O (1692 cm^{-1}, 6.31%), respectively.

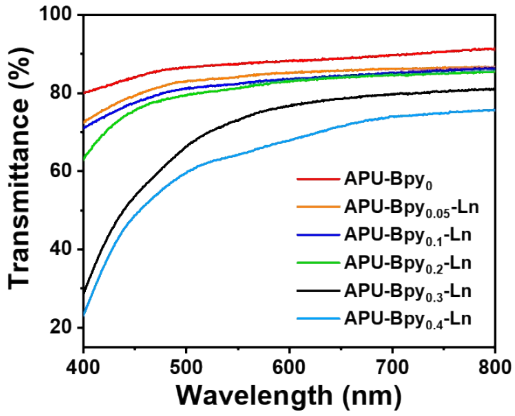

Figure S6. UV-vis transmittance spectra of various **APU-Bpy$_n$-Ln**.

n	0	0.05	0.1	0.2	0.3	0.4
Transmittance (%)	87.47	83.80	82.41	81.10	70.74	64.11

Table S2. The transmittance values of various **APU-Bpy$_n$-Ln** samples.

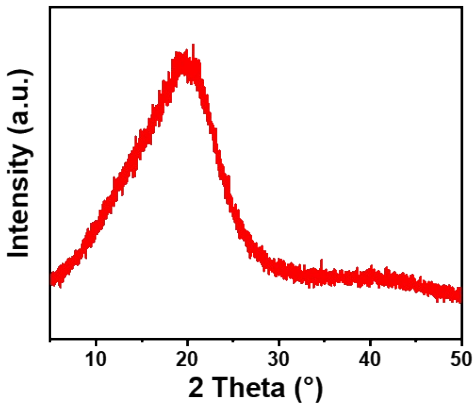

Figure S7. WAXD spectrum of the **APU-Bpy$_{0.1}$-Ln** elastomer.

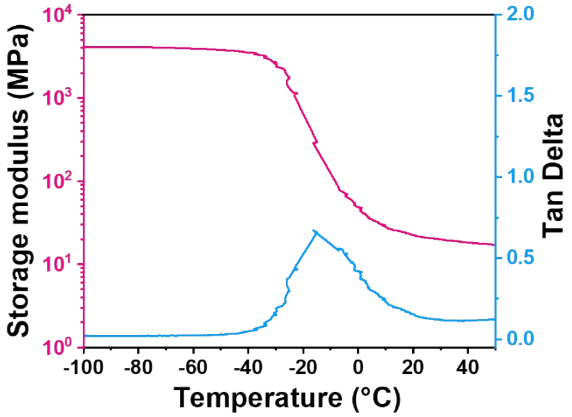

Figure S8. Temperature dependency of the tan δ and storage modulus (E′) of the three **APU-Bpy$_{0.1}$-Ln** elastomers.

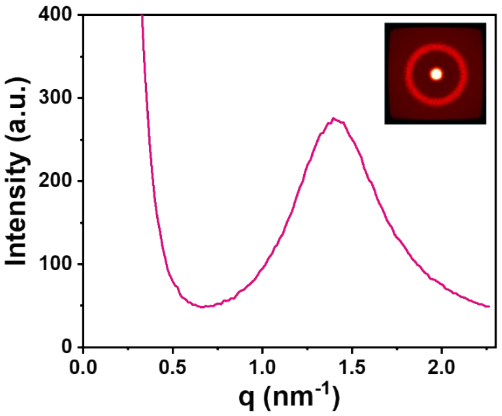

Figure S9. 1D-SAXS curves and 2D-SAXS images (inset) of **APU-Bpy$_{0.1}$-Tb** elastomers.

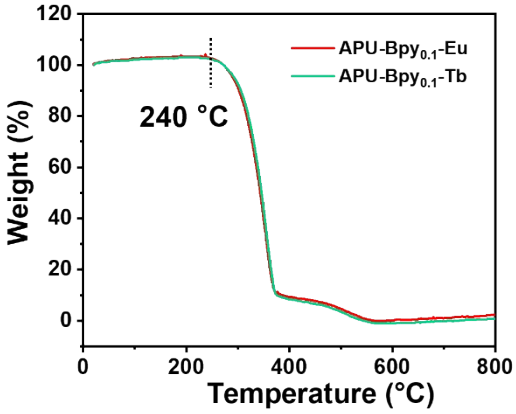

Figure S10. TGA curves of **APU-Bpy$_{0.1}$-Eu** and **APU-Bpy$_{0.1}$-Tb**.

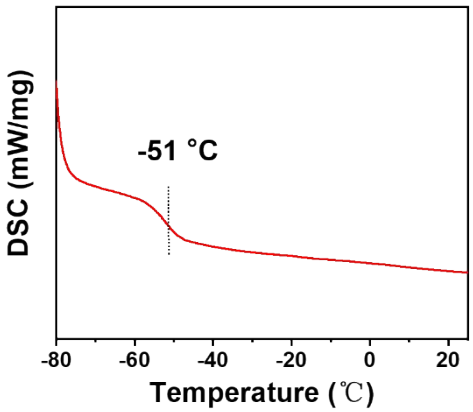

Figure S11. DSC curves of **APU-Bpy$_{0.1}$-Ln**.

Sample	Young's Modulus (MPa)	Ultimate tensile strength (MPa)	Elongation at break (%)	Toughness (MJ m^{-3})
APU-Bpy	7.33±0.63	9.84±0.71	2221±145	126.39±17.30
APU-$Bpy_{0.05}$-Ln	9.33±0.05	16.49±0.58	2345±33	199.20±5.89
APU-$Bpy_{0.1}$-Ln	16.88±0.26	38.34±2.16	2218±15	368.18±6.11
APU-$Bpy_{0.2}$-Ln	4.82±0.18	25.59±0.21	2620±168	256.03±18.97
APU-$Bpy_{0.3}$-Ln	3.06±0.55	15.94±0.27	2035±128	169.16±14.83
APU-$Bpy_{0.4}$-Ln	2.24±0.14	4.00±0.10	971±47	31.04±2.01

Table S3. Summary of mechanical properties of a range of **APU-Bpy_n-Ln** materials (stretch speed: 100 mm min^{-1}).

Sample name	Strength (MPa)	Toughness (MJ m^{-3})	Ref.
APU-$Bpy_{0.1}$-Ln	38.34±2.16	368.18±6.11	This work
HPU-$TPy_{0.25}$-Ln	11.21	133.35	18
Polymer-Phen-Ln^{3+}	2.27	8.4	15
Polymer-Phen-$Eu(tta)_3$	1.59	9.28	15
Eu-Ppdc	0.4	1.8	29
Ln^{3+}-Tpy-PPG	0.48	~10	16
PIB-Eu-TTA	0.58	6.27	17
H-PU-Ln	0.58	1.68	30
IPU-$Bpy_{0.15}$-Ln	1.76	42.25	14
TFE-HF-$QD_{1.0}$	1.8	19	32
Eu-to-IDA	6.1	6.4	33
p(HFBM-co-SBMA)	1.87	7.26	34
WPU-PD-0.45	25.91	102.80	31
CA-PDMS-1	1.04	5	35
TPE1%-AEA	0.37	~ 3	36
PDMS-DPBA-5000	0.28	11.76	37
PBA-co-PNMA	3.8	15	38

Table S4. Comparison of mechanical properties of **APU-$Bpy_{0.1}$-Ln** elastomer with synthetic room-temperature self-healing luminescent materials in the previous literatures.

Sample name	Strength (MPa)	Toughness (MJ m^{-3})	Ref.
APU-$Bpy_{0.1}$-Ln	38.34±2.16	368.18±6.11	This work
Fe-PPOU	11.9	139.8	39
MD-PU-SS	24.8	274.6	40
$PU_{3.8\text{-}80/20}$	34.1	127.3	41
SR-PU/SG	22.33	219.18	19
PU-S8L2	17.8	67.8	3
PU-SS-$DU_{0.04}$	14.08	64.6	42
PDM-2.5	29	104.1	43
PF_4M_6	0.69	31.41	44
M_7I_3-T-$PPG_{4:3}$	41.2	127.2	45
SPU-$UPy_{0.5}$: Zn = 1:1	14.15	47.57	46

Table S5. Comparison of mechanical properties of **APU-$Bpy_{0.1}$-Ln** with synthetic room-temperature self-healing non-luminescence elastomers reported previous.

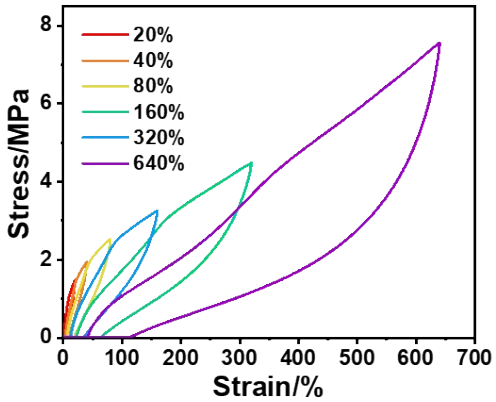

Figure S12. APU-$Bpy_{0.1}$-Ln was loaded and unloaded to different strains.

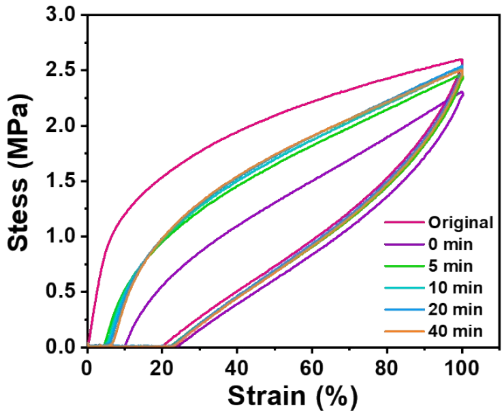

Figure S13. APU-Bpy$_{0.1}$-Ln was loaded and unloaded to100% strain with different rest time.

Sample	5 min	10 min	20 min	40 min
APU-Bpy$_{0.1}$-Ln	66.5%	68.3%	69.1%	70.1%

Table S6. W_2/W_1 values in cyclic loading and unloading with different rest time of **APU-Bpy$_{0.1}$-Ln** elastomers.

Time	Stain (%)	Stress (MPa)	Toughness (MJ m^{-3})	η (%)
5 min	188±3	4.88±0.16	6.58±0.35	1.79±0.09
10 min	373±4	6.61±0.17	18.58±0.58	5.05±0.16
30 min	750±9	9.57±0.08	48.66±1.23	13.22±0.33
24 h	1517±15	20.44±0.84	175.66±5.36	47.71±1.45

Table S7. Summary of self-healing efficiency of **APU-Bpy$_{0.1}$-Ln** after self-healing at room temperature for different times.

Temperature (°C)	Stain (%)	Stress (MPa)	Toughness (MJ m^{-3})	η (%)
RT	1517±15	20.44±0.84	175.66±5.36	47.71±1.45
40	1881±17	28.24±0.55	242.87±4.35	65.97±1.18
80	2183±20	33.96±1.67	355.95±5.39	98.68±1.46

Table S8. Summary of self-healed mechanical properties of **APU-Bpy$_{0.1}$-Ln** after different self-healing temperature for 24h.

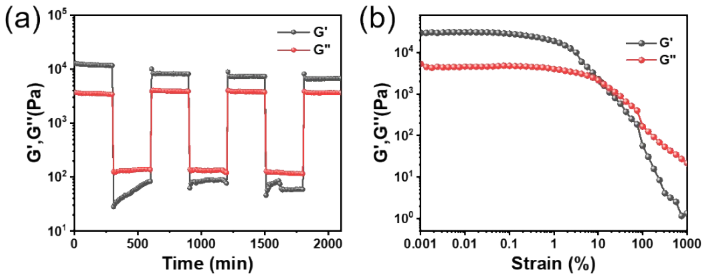

Figure S14. Rheological measurements of (a) alternate step strain tests (b) strain sweep tests and of storage modulus (G′) and loss modulus (G″) of **APU-Bpy$_{0.1}$-Ln**.

The results show that the elastomer is solid (G' > G") at 0.1% shear strain. However, when 100% high shear strain is carried out, the materials change from solid-state to liquid-state (G ' < G"), which indicates that the network of the elastomer is disrupted due to the fracture of the dynamic hydrogen bonding arrays and **Bpy-Ln** coordination bonds. After the strain recovers to 0.1%, the material recovers to the solid-state again (G' > G"), implying that the fractured dynamic bonds reconstructed, and the polymer network restores to its initial state. This phenomenon demonstrates the inherent dynamic properties of hydrogen bonding arrays and **Bpy-Ln** coordination interactions. At low strain amplitudes, the response is solid-like (G′ > G″), until the

yield point is reached where the G′ decreases and materials start to flow. These characteristics are typical of cross-linked polymer networks and soft glass materials.

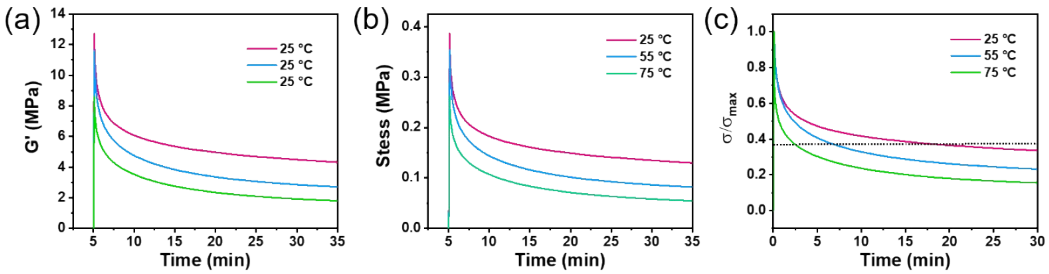

Figure S15. Relaxation curves of (a) modulus, (b) and (c) tensile strength of **APU-Bpy$_{0.1}$-Ln** tested at various temperatures with a stain of 3%.

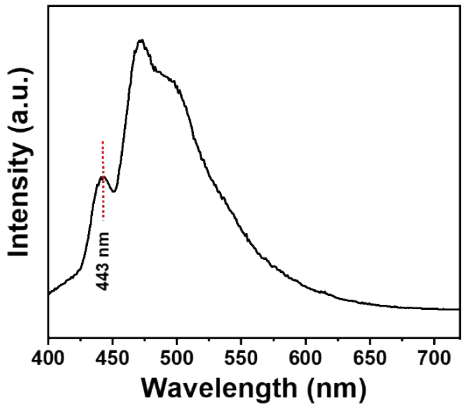

Figure S16. Phosphorescence curve of the **IPU-Bpy$_{0.15}$-Gd** excited at 316 nm at 77K.

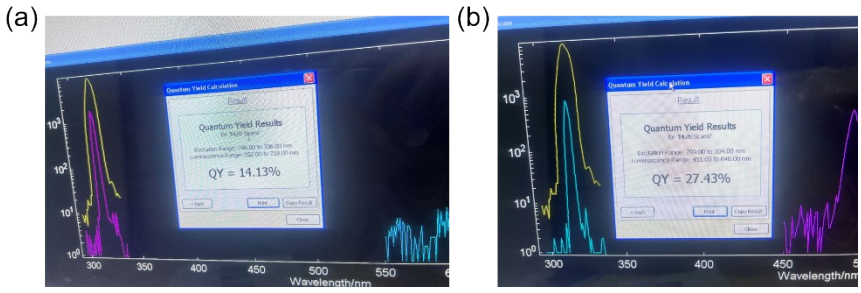

Figure S17. The absolute quantum yields of (a) **APU-Bpy$_{0.1}$-Eu** and (b) **APU-Bpy$_{0.1}$-Tb**.

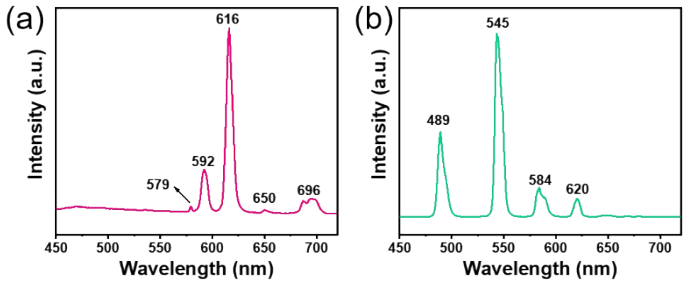

Figure S18. The emission spectra of (a) **APU-Bpy$_{0.1}$-Eu** and (b) **APU-Bpy$_{0.1}$-Tb** excited at 316 nm.

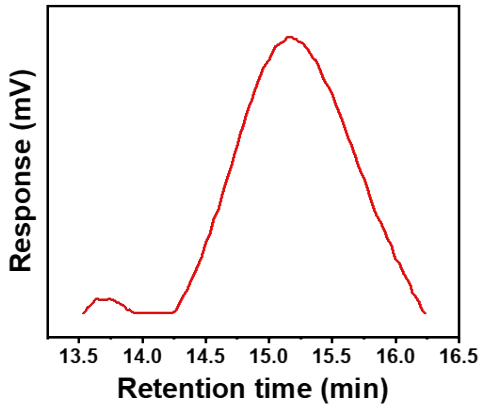

Figure S19. GPC curves of **APU-Bpy$_{0.1}$**.

References

[1] H. S. Guo, Y. Han, W. Q. Zhao, J. Yang, L. Zhang. Universally Autonomous Self-Healing Elastomer with High Stretchability. Nature Communications 11 (2020) 2037.